218 Transactions of Korean Society of Mechanical Engineers, Vol. 7, No. 2, pp. 218~225, 1983.

<Original>

Analytical Steady-State Jet Reattachment Model for a Wall-Attachment Fluid Amplifier†

Hyo Whan Chang*

(Received January 29, 1983)

側壁附着形 純流體素子의 噴流再接合모델에 관한 硏究

張 孝 煥

초 록

측벽부착형 순유체소자에서 제어입력이 존재할 때 2차원 난류제트가 오프셋된 경사면에 재접합하는 현상을 연구하였고 정상상태하의 재접합모델을 이론적으로 전개하였다.

순유체소자의 상하면이 제트의 확산에 미치는 영향을 조사하기 위하여 제트의 중심선에 따라 최대속도를 측정하였고, 그 결과에 따라 본 모델에 사용한 제트확산계수(σ)의 값은 자유제트의 것(σ=7.67)보다 큰 σ=10.5로 택하였다.

이론적 모델을 확증하기 위하여 제트의 재접합점과 변형각도에 관한 기존 논문에 보고된 실험적 연구결과와 비교하여 좋은 일치를 보았다.

1. Introduction

Digital fluidic devices or "fluid amplifiers" which utilize the "wall-attachment" phenomenon (called "wall-attachment fluid amplifiers") are used to implement logic circuits for a broad range of application.

Although extensive analytical and experimental work has been done on the basic jet reattachment phenomena in wall-attachment devices [1, 2, 3, 4, 5], no analytical model has been successful in accurately predicting the position of the jet reattachment in the presence of control flow.

In this study, an analytical steady-state jet reattachment model is developed for a wall-attachment fluid amplifier, which can predict the reattachment position of a two-dimensional, turbulent jet to an offset, inclined wall in the presence of control flow. The jet centerline axial velocity distribution in the semi-confined jet was measured to investigate the effect of the top and bottom plates on the effective jet spread in the test amplifier. Published experimental data on the steady-state jet reattachment distance [3] and jet deflection angle [9] are used to validate the analytical model.

† Presented at KSME Autumn Conference, 1982

* Member, Korea University

2. Analytical Model

2.1. Assumptions

Major assumptions made for the mathematical formulation of the model are as follows:

1) The jet flow is everywhere two-dimensional and incompressible.

2) Momentum interaction between the control and supply jets takes place in control volume 1 shown in Fig. 1. The deflected jet emerges from a "hypothetical nozzle" of width b_s, the exit of which is located at line $\overline{A_1A_2}$.

3) The velocity profiles at the exits of the control, supply, and hypothetical nozzles are uniform.

4) The supply jet velocity profile is describable by Goertler's turbulent-jet profile [6] and is not affected by the presence of the attachment wall. That is,

$$u=\frac{1}{2}\left[\frac{3J\sigma}{\rho(s+s_0)}\right]^{\frac{1}{2}}\operatorname{sech}^2\left(\frac{\sigma y}{s+s_0}\right) \qquad (1)$$

where J is the momentum flux per unit depth ($J\equiv\rho b_s U_s^2$), s_0 is the distance from the "hypothetical nozzle" exit to the "virtual origin" of the jet, and σ is the jet spread parameter.

5) The static pressure and wall-shear forces acting on control volume 2 in the vicinity of the reattachment point (Fig. 1) are negligible compared to the momentum flux of the jet.

6) The path of the entrainment streamline can be represented by the equation

$$r=k\sin\left(\frac{\theta}{c}\right) \qquad (2)$$

where k is a scale factor, θ is defined in Fig. 4, and $c=\frac{67}{90}$ [7].

7) The rate of fluid entrainment is the same on both sides of the jet.

8) The distance measured along the entrainment streamline is approximately equal to the distance measured along the jet centerline. That is, $s_e\cong s_f$ where $s_e\equiv\widehat{A_1E}$ and $s_f\equiv\widehat{A_0F}$ (see Fig. 1).

9) The angle included between the extended jet centerline and the wall is approximately the same as the one included between the extended entrainment streamline and the wall (γ in Fig. 1).

10) The supply and control jets retain their identity (i.e., there is no mixing of the jets) within control volume 1.

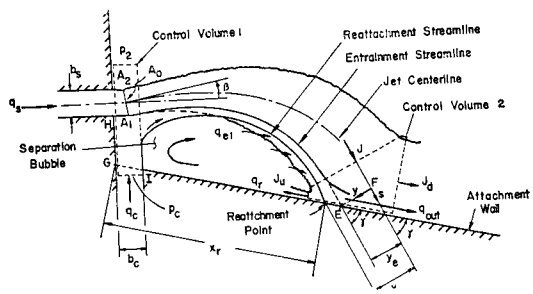

Fig. 1 Steady-state jet reattachment with control flow.

All variables in capital letters are dimensionless. Variables with the dimension of length are normalized with respect to supply nozzle width b_s. Variables with the dimension of area are normalized with respect to b_s since these variables are defined per unit depth in the present model. Flow rates are normalized with respect to the supply flow rate per unit depth q_s, and pressures are normalized with respect to supply jet dynamic pressure $\frac{1}{2}\rho U_s^2$ where $U_s\equiv q_s/b_s$.

2.2. Continuity Equation

The separation bubble is defined as the cavity enclosed between the entrainment streamline $\widehat{A_1E}$, attachment wall and lines $\overline{IG}$, $\overline{GH}$, and $\overline{HA_1}$ (Fig. 1). The flow balance in the separation bubble in the steady state is

$$Q_c=Q_{e1}-Q_r \qquad (3)$$

where Q_{e1} is the normalized flow rate entrained by the concave side of the jet, and Q_r is

the normalized return flow rate.

Using Eq. (1), Q_{e1} and Q_r can be written as

$$Q_{e1}=\frac{1}{q_s}\left(\int_0^\infty u\,dy\Big|_{s=s_e}-\frac{q_s}{2}\right)$$
$$=\frac{1}{2}\left(\sqrt{1+\frac{S_e}{S_0}}-1\right) \tag{4}$$

$$Q_r=\frac{1}{q_s}\int_{y_r}^\infty u\,dy\Big|_{s=s_e}$$
$$=\frac{1}{2}\sqrt{1+\frac{S_e}{S_0}}(1-T_r) \tag{5}$$

where $T_r\equiv\tanh\left(\frac{\sigma Y_r}{S_e+S_0}\right)$. (5a)

Combining Eqs. (3), (4) and (5) gives

$$Q_c=\frac{1}{2}\left(T_r\sqrt{1+\frac{S_e}{S_0}}-1\right). \tag{6}$$

2.3. Momentum Equation at Reattachment

Momentum equation for control volume 2 in the vicinity of the reattachment point (Fig. 1) can be written as [7]

$$J\cos\gamma=J_d-J_u$$
$$=\left|\rho\int_{-\infty}^{y_r}u^2\,dy-\rho\int_{y_r}^\infty u^2\,dy\right|_{s=s_e}. \tag{7}$$

Substituting Eq. (1) into the above gives

$$\cos\gamma=\frac{3}{2}T_r-\frac{1}{2}T_r^3. \tag{8}$$

Solving for T_r gives

$$T_r=2\cos\left(\frac{\pi+\gamma}{3}\right),\quad 0<\gamma<\frac{\pi}{2}. \tag{9}$$

2.4. Jet Deflection

The momentum equation in the logitudinal direction for control volume 1 (Fig. 1) is

$$(J+J_c)\cos\beta-\rho\frac{q_s^2}{b_s}=0 \tag{10}$$

where J_c is momentum flux of the control jet.

The momentum equation in the traverse direction is

$$(p_c-p_2)b_c=(J+J_c)\sin\beta-\rho\frac{q_c^2}{b_c} \tag{11}$$

where p_c is the control nozzle exit pressure and p_2 is the unattached side pressure. Eqs. (10) and (11), when combined and normalized, yield

$$\beta=\tan^{-1}\left[\frac{1}{2}(P_c-P_2)B_c+\frac{Q_c^2}{B_c}\right]. \tag{12}$$

The normalized control nozzle exit pressure P_c can be obtained by writing an energy equation between sections Z_1 and Z_2 in Fig.2. Losses due to an abrupt change in the direction of the control flow are accounted for through use of a minor loss coefficient K_L, i.e.,

$$P_c=P_{cb}+Q_c^2\left(\frac{1}{A_c^2}+\frac{K_L-1}{B_c^2}\right) \tag{13}$$

where P_{cb} is the normalized pressure in section Z_2, and A_c is the normalized area of the control flow passage in the section (see Fig. 3). If $A_c\geq B_c$, the term A_c in the above equation must be replaced by B_c, since the control jet retains its width B_c within control volume 1. A_c can be obtained geometrically from Fig. 3, i.e.,

$$A_c=\frac{1}{2}B_c\sin\beta+\left(D_1+\frac{1}{2}\right.$$
$$\left.+B_c\tan\alpha_1\right)\cos\beta-\frac{1}{2}. \tag{14}$$

Based on pressure distribution measurements along the attachment wall [5], it is assumed that $P_{cb}=(P_1+P_2)/2$ where P_1 is the normalized average pressure in the separation bubble. P_1 can be obtained from Euler's equation written in the direction (y) normal to the jet centerline to calculate the pressure difference Δp across the jet [4, 8, 9]. Referring to Fig.2,

$$P_1\cong P_2-\frac{2}{R_c}. \tag{15}$$

The average pressure p_2 in region 2 (Fig. 2) can be obtained from steady-state flow rate balance in the region, i.e.,

$$\Sigma q=(q_b+q_{v2}-q_{02})-q_{e2}=0 \tag{16}$$

where

$$q_b=b_b\sqrt{\frac{-2p_2}{\rho}},\quad q_{v2}=b_{v2}\sqrt{\frac{-2p_2}{\rho}}$$

$$q_{02}=-w_{02}\sqrt{\frac{-2p_2}{\rho}},\quad q_{e2}=\int_0^\infty u\,dy\Big|_{s=s_e}-\frac{q_s}{2}.$$

Here, it is assumed that the discharge coeffi-

cients for the above equations are equal to unity and the output 2 is open to the ambient. Eq. (16), when rearranged and normalized, yields

$$P_2=-\left[\frac{Q_{e2}}{B_b+B_{v2}+W_{02}}\right]^2 \tag{17}$$

where $Q_{e2}\equiv\frac{q_{c2}}{q_s}=\frac{1}{2}\left(\sqrt{1+\frac{S_s}{S_0}}-1\right)$.

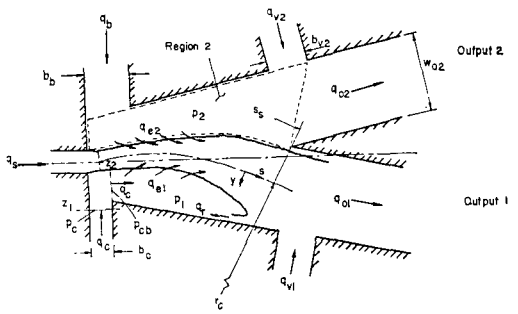

Fig. 2 Overall steady-state flow model for a wall-attachment fluid amplifier.

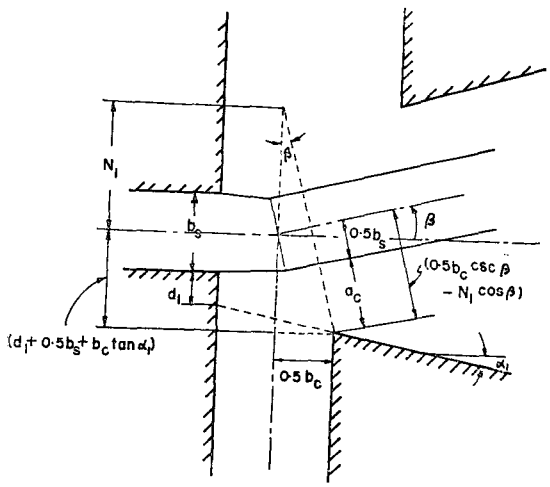

Fig. 3 Control flow passage width.

2.5. Geometric Relations

Referring to Fig. 4, the following geometric relations can be written in normalized form:

$$R_e=K\sin\left(\frac{\theta_e}{c}\right) \tag{18}$$

$$\alpha_1+\gamma=\zeta_e+\theta_e-\beta \tag{19}$$

$$E_1=D_1+X_1\sin\alpha_1+\frac{1}{2}(1-\cos\beta) \tag{20a}$$

or $$E_1=R_e\sin(\theta_e-\beta-\alpha_1)\sec\alpha_1 \tag{20b}$$

$$X_1=\frac{1}{2}(B_c+\sin\beta)\sec\alpha_1 \tag{21}$$

$$X_2=R_e\cos(\theta_e-\beta)\sec\alpha_1 \tag{22}$$

$$X_e=X_1+X_2. \tag{23}$$

Also, from Fig. 4,

$$ds=[(rd\theta)^2+(dr)^2]^{\frac{1}{2}} \tag{24}$$

Eqs. (2) and (24), when combined and integrated, yield

$$S_e=K\int_0^{\theta_e/c}\left[1-(1-c^2)\sin^2\left(\frac{\theta}{c}\right)\right]^{\frac{1}{2}}d\left(\frac{\theta}{c}\right). \tag{25}$$

The above equation is an elliptic integral of the second kind which is well tabulated. For computional purposes, S_e may be approximated as [4]

$$S_e\cong K\left[0.62\left(\frac{\theta_e}{c}\right)+0.38\sin\left(\frac{\theta_e}{c}\right)\right]. \tag{25a}$$

From Fig. 4 and Eq. (2)

$$\zeta_e=\tan^{-1}\left(\frac{rd\theta}{dr}\right)_{\theta=\theta_e}=\tan^{-1}\left(c\tan\frac{\theta_e}{c}\right) \tag{26}$$

Referring to Figs. 1 and 4,

$$X_r=X_e-(Y_r-Y_e)\csc\gamma \tag{27}$$

where Y_e can be obtained from $\int_0^{y_e}u\,dy\Big|_{s=s_e}=\frac{1}{2}U_sb_s$, i.e.,

$$Y_e=\left(\frac{S_e+S_0}{\sigma}\right)\tanh^{-1}\sqrt{\frac{S_0}{S_e+S_0}}. \tag{28}$$

Substituitng Y_e and Y_r from Eq. (5a) into Eq. (27) gives

$$X_r=X_e-\frac{S_e+S_0}{\sigma}\left[\tanh^{-1}T_r-\tanh^{-1}\sqrt{\frac{S_0}{S_e+S_0}}\right]\csc\gamma. \tag{29}$$

Referring to Figs. 4 and 5, the normalized radius R_{es} of the circular arc which is tangent to the entrainment streamline at point A_1 can be expressed as

$$R_{es}\equiv\frac{r_{es}}{b_s}=\frac{1}{b_s}\left[\frac{ds}{d(\theta+\zeta)}\right]_{\theta=0}=\frac{K}{2c}. \tag{30}$$

The average radius of curvature of the jet centerline is assumed to be the radius r_c of the circular arc which is tangent to the jet centerline at the hypothetical nozzle exit and which passes at a distance y_p from point P (Fig. 5). That is,

$$R_c=R_{es}+\frac{1}{2}\left[1+\frac{\left(\frac{1}{2}-Y_p\right)\left(2R_{es}+\frac{1}{2}-Y_p\right)}{R_{es}(\cos 2\theta_p-1)-\frac{1}{2}+Y_p}\right] \quad (31)$$

where

$$Y_p=\left(\frac{S_p+S_0}{\sigma}\right)\tanh^{-1}\sqrt{\frac{S_0}{S_p+S_0}}.$$

From Fig. 5, the following relations can also be written in normalized form:

$$\eta_1=\tan^{-1}\left[\frac{D_s-\frac{1}{2}B_c-\left(R_{es}+\frac{1}{2}\right)\sin\beta}{\left(R_{es}+\frac{1}{2}\right)\cos\beta+D_3}\right] \quad (32)$$

$$\eta_2=\tan^{-1}\left[\frac{D_s-\frac{1}{2}B_c-R_c\sin\beta}{R_c\cos\beta+D_3}\right] \quad (33)$$

$$\theta_p=\frac{1}{2}(\beta+\eta_1) \quad (34)$$

$$S_p=2R_{es}\theta_p \quad (35)$$

$$S_s=R_c(\beta+\eta_2) \quad (36)$$

2.6. Numerical Computatron Procedure

Given the geometry and control flow rate Q_c, any steady-state value of a variable can be obtained by numerically solving the basic equations and the geometric relations derived above. The following are the list of the basic equations and the geometric relations to be solved: Eqs. (6), (9), (12) through (15), (17) through (23), (25a), (26), (29) through (36).

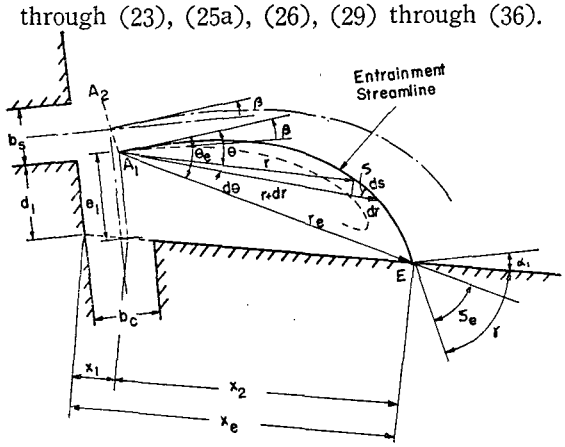

Fig. 4 Geometry for the steady-state jet reattachment model.

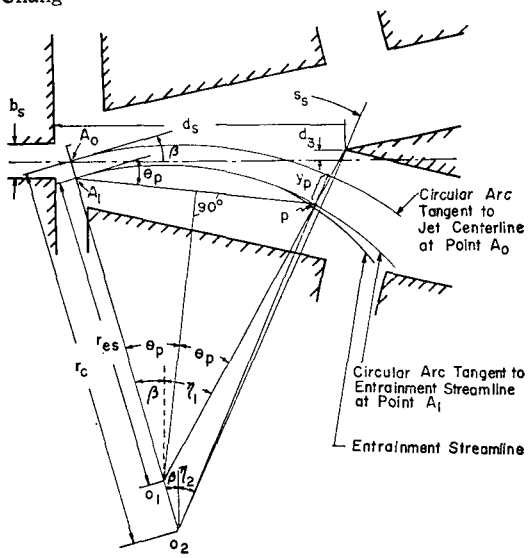

Fig. 5 Geometry of jet centerline curvature.

3. Experimental Apparatus and Procedure

Fig. 6 is a plan view of a large-scale test amplifier. The major components of the test model were a base plate, a cover plate, and movable internal blocks. The supply nozzle width (b_s) was fixed at 2.54 mm, which resulted in an aspect ratio (AR) of 3.1. All measurements were conducted with a supply total pressure of 25.4cm H_2O and 50.8cm H_2O. The Reynolds numbers are approximately 9.8×10^3 and 1.4×10^4, respectively. Jet centerline axial velocities in the semi-confined jet (no side walls and splitter) were "computed" from the total pressure measurements along the jet axis, assuming the static pressure was constant

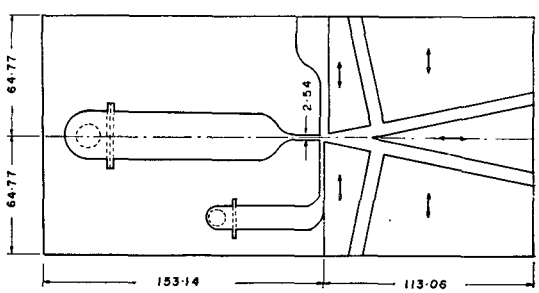

Fig. 6 Plan view of large-scale test amplifier.

throughout the jet field. The total pressure was measured midway between the top and bottom plates with a standard total pressure probe (1.65mm O.D.) mounted on a traverse mechanism and a Meriam manometer.

4. Results and Discussion

4.1. Jet Spread Parameter

Goetrtler's jet velocity profile [6] given by Eq. (1) has an experimentally derived parameter σ which is called a jet spread parameter. A value of $\sigma=7.67$ was found for a two-dimensional, turbulent free jet [11]. However, that value of σ does not hold for the semi-confined jet because the top and bottom plates reduce the jet entrainment.

Fig. 7 shows jet centerline axial velocity distributions in the semi-confined jet. The measured velocities are normalized with respect to continuity averaged velocity U_s at the supply nozzle exit plane. The uncertainty in these measurements is of the order of one percent of full scale $\left(\frac{u_c}{U_s}=1.0\right)$. Due to the boundary layer development in the nozzle, u_c/U_s is greater than one in the "zone of flow establishment". Goertler's theory [6] with $\sigma=10.5$ yields best match with the experimental data for $s/b_s\geq25$. Since the constant-velocity "potential core" region is not considered in Goertler's theory, the agreement between his theory and the experimental data is generally poor in the "zone of flow establishment". For the range of $4<s/b_s<15$, $\sigma=20$ yields better agreement with the experimental data than $\sigma=10.5$.

Although it is possible to use Albertson's two-dimensional theory [6] (dashed line in Fig. 7) in the model, the resulting equations will be unnecessarily complex and difficult to solve. Two previous studies [7, 12] provide justification for using Geortler's profile in the present study.

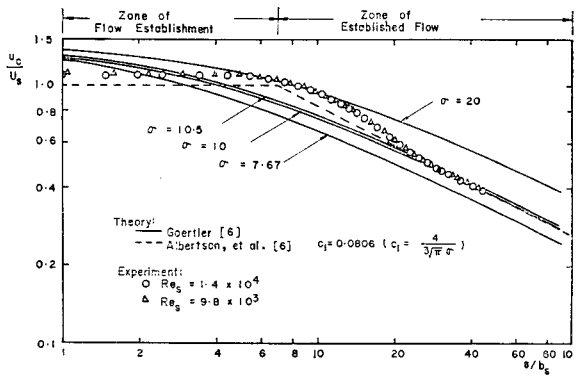

Fig. 7 Jet centerline axial velocity distributions in the semi-confined jet ($AR=3.1$).

4.2. Comparison of Analytical Predictions with Experimental Data

Fig. 8 shows the variations of steady-state reattachment distance with control flow rate for offset $D_1=0.5$ and wall angle $\alpha_1=15°$. Since Goertler's theory with a single value of σ does not correctly predict the mersured centerline velocity for the entire range of s, steady-state jet reattachment distances were calculated using two values of σ (i.e., $\sigma=10.5$ and $\sigma=20$). With $\sigma=10.5$, analytically predicted reattachment distances are in good agreement with experimental data due to Kimura and Mitsuoka [3].

Analytical predictions of two other investigators [4, 8] are also compared with the experimental data in Fig. 8. Goto and Drzewiecki [8] used a value of $\sigma=10$ in their model and Epstein [4] used a value of $\sigma=31.5$. Since the value of $\sigma=31.5$ is unusually large, steady-state jet reattachment distances were also calculated by the author using Epstein's model with $\sigma=10.5$. Predictions using the present model ($\sigma=10.5$) correlate significantly better with the experimental data than do those of other investigators.

Fig. 9 shows the variation of jet deflection

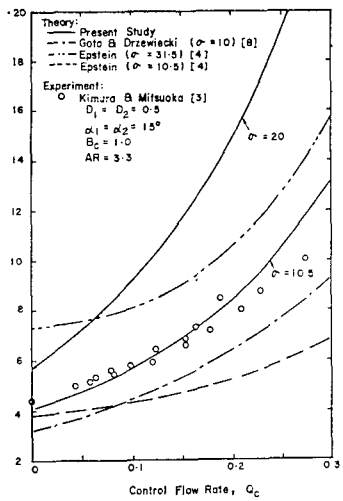

Fig. 8 Variation of steady-state reattachment distance with control flow rate for $D_1=0.5$ and $\alpha_1=15°$.

angle with control flow rate for offset $D_1=0.482$ and wall angle $\alpha_1=15°$. Analytical predictions using the present model correlate significantly better with Lush's experimental data [9] than do those of other investigators [2, 3, 8]. The value of minor loss coefficient K_L used in the present model was chosen to be unity by matching a predicted jet deflection angle with a particular measured value ($\beta=0.08$ rad.) due to Lush [9] for $Q_c=0.25$, D_1

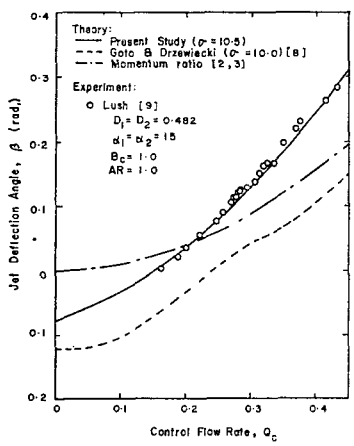

Fig. 9 Variation of jet deflection angle with control flow rate for $D_1=0.482$ and $\alpha_1=15°$.

$=0.482$, and $\alpha_1=15°$. However, as shown in Figs. 9 and 10, the present model predictions agree well with the experimental data [9] for the entire range of the control flow rate used and for the wall offset D_1 of 0.107 to 0.732.

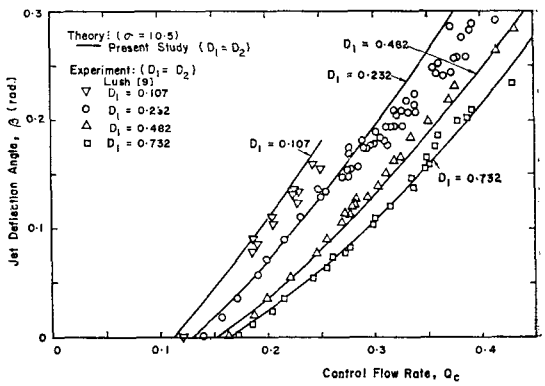

Fig. 10 Variation of jet deflection angle with control flow rate for D_1 of 0.107 to 0.732, $\alpha_1=15°$, and $B_c=1.0$.

5. Conclusions

A steady-state jet reattachment model was developed for a wall-attachment fluid amplifier, which is capable of accurately predicting the reattachment position of a two-dimentional, turbulent jet to an offset, inclined wall in the presence of control flow.

It was found that the value of jet spread parameter σ for the semi-confined jet in the test amplifier is larger than a value of $\sigma=7.67$ for a two-dimensional, turbulent free jet. With $\sigma=10.5$, analytically predicted jet reattachment distances and jet deflection angles are in good agreement with published experimental data [3, 9].

This steady-state model can be used to determine the inside geomentry (e.g., offset, wall angle and length, etc.) of a wall-attachment fluid amplifier and also used for one to understand the basic switching mechanism in a wall-attachment device.

References

1. N.C. Sher, Jet Attachment and Switching in Bistable Fluid Amplifiers, ASME Paper 64—FE—19, 1964.
2. M.P. Wilson, The Switching Process in Bistable Fluid Amplifiers, ASME Paper 69—Flcs—28, 1969.
3. M. Kimura and T. Mitsuoka, Analysis and Design of Wall Attachment Devices by a Jet Model of Unsymmetrical Velocity Profile, First IFAC Symp. on Fluidics Proc., Paper A2, 1968.
4. M. Epstein, Theoretical Investigation of the Switching Mechanism in a Bistable Wall Attachment Fluid Amplifier, Air Force Avionics Laboratory TR—70—198, Ohio, 1970.
5. T. Wada, M. Takagi, and T. Shimizu, Effects of a Splitter and Vents on a Reattaching Jet and Its Switching in Wall-Reattachment Fluidic Devices, HDL Fluidic State-of-the-Art Symp., Vol. 1, pp. 499—554, 1974.
6. J.M. Kirshner, Jet Flows, Fluidics Quarterly, Vol. 1, No. 3, pp. 33—46, 1968.
7. C. Bourque, Reattachment of Two Dimensional Jet to an Adjacent Flat Plate, Advances in Fluidics, Ed. F.T. Brown, pp. 192—204, ASME, New York, 1967.
8. J.M. Goto and T.M. Drzewiecki, Fluerics 32. An Analytical Model for the Response of Flueric Wall Attachment Amplifiers, HDL TR—1598, Washington, D.C., 1972.
9. P.A. Lush, The Development of a Theoretical Model for the Switching Mechanism of a Wall Attachment Fluid Amplifier, Ph. D. dissertation, University of Bristol, U.K., 1968.
10. H.W. Chang, Dynamic Analysis of a Monostable Fluid Amplifier, Ph. D. dissertation, Oklahoma State University, U.S.A., 1978.
11. H. Schlichting, Boundary-Layer Theory, 6th. Ed., McGraw-Hill, New York, 1968.
12. M.R. Ozgu and A.H. Stenning, Theoretical Study of the Switching Dynamics of Bistable Fluidic Amplifiers with Low Setbacks, ASME Paper 71—WA/Flcs—6, 1971.